Direct links between dynamical, thermodynamic, and structural properties of liquids: Modeling results

L. Wang,[1] C. Yang,[1] M. T. Dove,[1] Yu. D. Fomin,[2] V. V. Brazhkin,[2] and K. Trachenko[1]
[1]*School of Physics and Astronomy, Queen Mary University of London, Mile End Road, London E1 4NS, United Kingdom*
[2]*Institute for High Pressure Physics, RAS, 142190 Moscow, Russia*
(Received 19 October 2016; published 7 March 2017)

We develop an approach to liquid thermodynamics based on collective modes. We perform extensive molecular-dynamics simulations of noble, molecular, and metallic liquids, and we provide direct evidence that liquid energy and specific heat are well-described by the temperature dependence of the Frenkel (hopping) frequency. The agreement between predicted and calculated thermodynamic properties is seen in the notably wide range of temperature spanning tens of thousands of Kelvin. The range includes both subcritical liquids and supercritical fluids. We discuss the structural crossover and interrelationships between the structure, dynamics, and thermodynamics of liquids and supercritical fluids.

DOI: 10.1103/PhysRevE.95.032116

I. INTRODUCTION

It is an interesting fact that the liquid state has proven to be difficult to describe by theory throughout the history of condensed-matter research [1–12]. The problem extends beyond condensed matter and exists in other areas where strong interactions are combined with dynamical disorder, such as field theory.

In a weakly interacting system such as a dense gas, the potential energy is much smaller than the kinetic energy. These systems are amenable to perturbation treatment giving corrections to the noninteracting case [5]. Perturbation approaches have been widely explored to calculate liquid thermodynamic properties, but they have not been able to agree with experiments. For example, the analysis of tractable models such as van der Waals or hard-spheres systems returns the gaslike result for the liquid constant-volume specific heat $c_v = \frac{3}{2}k_B$ [12–14]. This is in contrast to experimental results showing that c_v of monatomic liquids close to the melting point is nearly identical to the solidlike result, $c_v = 3k_B$, and decreases to about $2k_B$ at high temperature [15,16]. As expected on general grounds, the perturbation approach does not work for strongly interacting systems.

Strong interactions are successfully treated in solids, crystals, or glasses, where the harmonic model is a good starting point and gives most of the vibrational energy. However, this approach requires fixed reference points around which the energy expansion can be made. With small vibrations around mean atomic positions, solids meet this requirement but liquids seemingly do not: the ability of liquids to flow implies that the reference lattice is nonexistent.

Therefore, liquids seemingly have no simplifying features such as small interactions of gases or small displacements of solids [12]. In other words, liquids have no small parameter. One might adopt a general approach that does not rely on approximations and seek to directly calculate the liquid energy for a model system in which interactions and structure are known. This meets another challenge: because the interactions are both strong and system-dependent, the resulting energy and other thermodynamic functions will also be strongly system-dependent, precluding their calculation in general form and understanding using basic principles, in contrast to solids and gases [12]. Consistent with this somewhat pessimistic view, the discussion of liquid thermodynamic properties has remained scarce. Indeed, physics textbooks have very little, if anything, to say about liquid specific heat, including textbooks dedicated to liquids [1–12].

As recently reviewed [17], emerging evidence advances our understanding of the thermodynamics of the liquid state. The starting point is the early theoretical idea of Frenkel [1], who proposed that liquids can be considered as solids at times smaller than liquid relaxation time, τ, the average time between two particle rearrangements at one point in space. This implies that phonons in liquids will be similar to those in solids for frequencies above the Frenkel frequency ω_F:

$$\omega > \omega_F = \frac{1}{\tau}. \tag{1}$$

The above argument predicts that liquids are capable of supporting shear modes, the property hitherto attributable to solids only, but only for frequencies above ω_F.

We note that low-frequency modes in liquids, sound waves, are well-understood in the hydrodynamic regime $\omega\tau < 1$ [18], however Eq. (1) denotes a distinct, solidlike elastic regime of wave propagation where $\omega\tau > 1$. In essence, this suggests the existence of a cutoff frequency ω_F above which particles in the liquid can be described by the same equations of motion as in, for example, solid glass. Therefore, liquid collective modes include both longitudinal and transverse modes with frequency above ω_F in the solidlike elastic regime and one longitudinal hydrodynamic mode with frequency below ω_F (the shear mode is nonpropagating below frequency ω_F, as discussed below).

Recall the earlier textbook assertion [12] that a general thermodynamic theory of liquids cannot be developed because liquids have no small parameter. How is this fundamental problem addressed here? According to Frenkel's idea, liquids behave like solids with small oscillating particle displacements serving as a small parameter. Large-amplitude diffusive particle jumps continue to play an important role, but they do not destroy the existence of the small parameter. Instead, the jumps serve to modify the phonon spectrum: their frequency, ω_F, sets the minimal frequency above which the small-parameter description applies and solidlike modes propagate.

It has taken a long time to verify this picture experimentally. The experimental evidence supporting the propagation of high-frequency modes in liquids currently includes inelastic x-ray, neutron, and Brillouin scattering experiments, but most important evidence is recent and follows the deployment of powerful synchrotron sources of x rays [19–35].

Early experiments detected the presence of high-frequency longitudinal acoustic propagating modes and mapped dispersion curves that bore a striking resemblance to those in solids [19]. These and similar results were generated at a temperature just above the melting point. The measurements were later extended to high temperatures considerably above the melting point, confirming the same result. It is now well established that liquids sustain propagating modes with wavelengths extending down toward interatomic separations, comparable to the wave vectors of phonons in crystals at the Brillouin zone boundaries [20–31]. More recently, the same result has been asserted for supercritical fluids [24,30,31]. Importantly, the propagating modes in liquids include acoustic transverse modes. These were first seen in highly viscous fluids (see, e.g., Refs. [32,33]), but they were then studied in low-viscosity liquids on the basis of positive dispersion [20–22] (the presence of high-frequency transverse modes increases sound velocity from the hydrodynamic to the solidlike value). These studies included water [34], where it was found that the onset of transverse excitations coincides with the inverse of liquid relaxation time [35], as predicted by Frenkel [1].

More recently, high-frequency transverse modes in liquids were directly measured in the form of distinct dispersion branches and verified on the basis of computer modeling [25–29], and the striking similarity between dispersion curves in liquids and their crystalline (polycrystalline) counterparts was noted. We note that the contribution of high-frequency modes is particularly important for liquid thermodynamics because these modes make the largest contribution to the energy due to quadratic density of states.

The above discussion calls for an important question about liquid thermodynamics. In solids, collective modes (phonons) play a central role in the theory, including the theory of thermodynamic properties. Can collective modes in liquids play the same role, in view of the earlier Frenkel proposal and recent experimental evidence? We started exploring this question [36] just before the high-frequency transverse modes were directly measured, and subsequently we developed it in a number of ways [17]. This involves calculating the liquid energy as the phonon energy where transverse modes propagate above ω_F in Eq. (1).

The main aim of this paper is to provide direct computational evidence of the phonon theory of liquid thermodynamics and its predictions. We achieve this by calculating the liquid energy and ω_F in extensive molecular-dynamics simulations. In the next section, we briefly discuss the main steps involved in calculating the liquid energy. We then proceed to calculate the liquid energy and Frenkel frequency independently from molecular-dynamics simulations using several methods that agree with each other. We do this for three systems chosen from different classes of liquids: noble, metallic, and molecular, and we find good agreement between predicted and calculated results in the wide range of temperature and pressure. The range includes both subcritical liquids and the supercritical state below the Frenkel line where transverse waves propagate. We calculate and analyze liquid energy and c_v using several different methods. Finally, we discuss how our results offer insights into interrelationships between structure, dynamics, and thermodynamics in liquids and supercritical fluids.

II. PHONON APPROACH TO LIQUID THERMODYNAMICS

A. Calculating liquid energy

We summarize the main result of the calculation of the liquid energy on the basis of propagating modes. A detailed discussion can be found in a recent review [17].

According to the previous discussion, the propagating modes in liquids include two transverse modes propagating in the solidlike elastic regime with frequency $\omega > \omega_F$. The energy of these modes, together with the energy of the longitudinal mode, gives the liquid vibrational energy. In addition to vibrations, particles in the liquids undergo diffusive jumps between quasiequilibrium positions, as discussed above. Adding the energy of these jumps to the phonon energy in the Debye model gives the total energy of thermal motion in the liquid [17,36]:

$$E_T = NT\left[3 - \left(\frac{\omega_F}{\omega_D}\right)^3\right], \tag{2}$$

where N is the number of particles, ω_D is the transverse Debye frequency, and the subscript T refers to thermal motion. Here and below, $k_B = 1$.

At low temperature, $\tau \gg \tau_D$, where τ_D is the Debye vibration period, or $\omega_F \ll \omega_D$. In this case, Eq. (2) gives the specific heat $c_v = \frac{1}{N}\frac{dE}{dT}$ close to 3, which is the solidlike result. At high temperature when $\tau \to \tau_D$ and $\omega_F \to \omega_D$, Eq. (2) gives c_v close to 2. The decrease of c_v from 3 to 2 with temperature is consistent with experimental results in monatomic liquids [15,16]. The decrease of c_v is also seen in complex liquids [37].

Equation (2) attributes the experimental decrease of c_v with temperature to the reduction of the number of transverse modes above the frequency $\omega_F = \frac{1}{\tau}$. The comparison of this effect with experiments can be more detailed if c_v is compared in the entire temperature range where it decreases from 3 to 2. This meets the challenge that ω_F in Eq. (2) is not directly available in the cases of interest. $\omega_F(\tau)$ is measured in dielectric relaxation or NMR experiments in systems responding to electric or magnetic fields only. These liquids are often complex and do not include simple model systems that are widely studied theoretically, such as liquid Ar. Importantly, the range of measured ω_F does not extend to high frequency comparable to ω_D, and it is in this range where liquid c_v undergoes an important change from 3 to 2 as discussed above. ω_F can be calculated from the Maxwell relationship $\omega_F = \frac{G_\infty}{\eta}$, where G_∞ is the instantaneous shear modulus and η is the viscosity taken from a different experiment [17]. More recently, it has been suggested [39] that taking the shear modulus at a finite high frequency (rather than infinite frequency) agrees better with the modeling data. Apart from rare estimations [38,39], G_∞ is not available. In practice, the comparison of experimental c_v and c_v predicted as $\frac{dE}{dT}$ with E given by

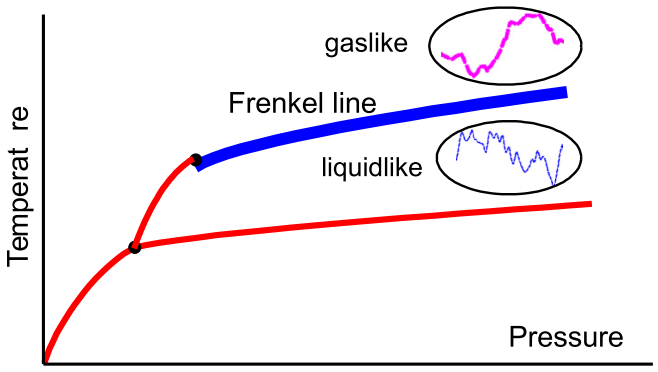

FIG. 1. The Frenkel line in the supercritical region. Particle dynamics includes both oscillatory and diffusive components below the line, and it is purely diffusive above the line. Below the line, the system is able to support rigidity and transverse modes at high frequency. Above the line, particle motion is purely diffusive, and the ability to support rigidity and transverse modes is lost at all available frequencies. Crossing the Frenkel line from below corresponds to the transition between the "rigid" liquid to the "nonrigid" gaslike fluid.

Eq. (2) is done by keeping G_∞ as a free parameter, obtaining a good agreement between experimental and predicted c_v and observing that G_∞ lies in the range of several GPa typical for liquids [17,36]. In the past few years, Eq. (2) and its extensions to include the phonon anharmonicity and quantum effects of phonon excitations were shown to account for the experimental c_v of over 20 different systems, including metallic, noble, molecular, and network liquids [17].

In view of the persisting problem of liquid thermodynamics, it is important to test Eq. (2) directly by linking the liquid energy (c_v) on one hand and ω_F on the other and testing the theory in a precise way. This, together with achieving consistency with other approaches to calculate the liquid energy, is one of the objectives of this study. Importantly, this program includes supercritical fluids as well as subcritical liquids, as discussed below.

B. Thermodynamics of supercritical fluids

If the system is below the critical point (see Fig. 1), the temperature increase eventually results in boiling and the first-order transition, with c_v discontinuously decreasing to about $\frac{3}{2}$ in the gas phase. The intervening phase transition excludes the state of the liquid where c_v can gradually reduce to $\frac{3}{2}$ and where interesting physics operates. However, this becomes possible above the critical point. This brings us to the interesting discussion of the supercritical state of matter. Theoretically, little is known about the supercritical state, apart from the general assertion that supercritical fluids can be thought of as high-density gases or high-temperature fluids whose properties change smoothly with temperature or pressure and without qualitative changes of properties. This assertion followed from the known absence of a phase transition above the critical point. We have recently proposed that this picture should be modified, and that a new line, the Frenkel line (FL), exists above the critical point and separates two states with distinct properties (see Fig. 1) [13,14,40,41]. Physically, the FL is not related to the critical point, and it exists in systems where the critical point is absent.

The main idea of the FL lies in considering how the particle dynamics changes in response to pressure and temperature. Recall that particle dynamics in the liquid can be separated into solidlike oscillatory and gaslike diffusive components. This separation applies equally to supercritical fluids as it does to subcritical liquids. Indeed, increasing temperature reduces τ, and each particle spends less time oscillating and more time jumping; increasing pressure reverses this and results in the increase of time spent oscillating relative to jumping. Increasing temperature at constant pressure or density (or decreasing pressure at constant temperature) eventually results in the disappearance of the solidlike oscillatory motion of particles; all that remains is the diffusive gaslike motion. This disappearance represents the qualitative change in particle dynamics and gives the point on the FL in Fig. 1. Most important system properties change qualitatively either on the line or in its vicinity [13,14,40,41]. In a given system, the FL exists at arbitrarily high pressure and temperature, as does the melting line.

Quantitatively, the FL can be rigorously defined by pressure and temperature at which the minimum of the velocity autocorrelation function (VAF) disappears [14]. Above the line defined in such a way, velocities of a large number of particles stop changing their sign, and particles lose the oscillatory component of motion. Above the line, the VAF is monotonically decaying as in a gas [14]. For the purposes of this discussion, the significance of the FL is that the phonon approach to liquids and Eq. (2) apply to supercritical fluids below the FL to the same extent as they apply to subcritical liquids. Indeed, the presence of an oscillatory component of particle motion below the FL implies that τ is a well-defined parameter and that transverse modes propagate according to Eq. (1). The ability of the supercritical system to sustain solidlike rigidity at a frequency above ω_F suggested the term "rigid" liquid to differentiate it from the "nonrigid" gaslike fluid above the FL [13,14].

Therefore, the FL separates the supercritical state into two states where transverse modes can and cannot propagate. This is supported by direct calculation of the current correlation functions [42] showing that propagating and nonpropagating transverse modes are separated by the Frenkel line. Interestingly, Eq. (2) can serve as a thermodynamic definition of the FL: the loss of the oscillatory component of particle motion at the FL corresponds approximately to $\tau \to \tau_D$ (here, τ_D refers to the Debye period of transverse modes) or $\omega_F \to \omega_D$. According to Eq. (2), this gives c_v of about 2. Using the criterion $c_v = 2$ gives the line that is in remarkably good agreement with the line obtained from the VAF criterion above [14].

III. SIMULATION DETAILS

We have considered liquids from three important system types: noble Ar, molecular CO_2, and metallic Fe. We have used the molecular-dynamics (MD) simulation package DL_POLY [43] and simulated systems with 4576–8000 particles with periodic boundary conditions. The interatomic potential for Ar is the pair Lennard-Jones potential [44], known

to perform well at elevated pressure and temperature. For CO_2 and Fe, we have used interatomic potentials that were optimized and tested in the liquid state at high pressure and temperature. The potential for CO_2 is the rigid-body nonpolarizable potential based on a quantum chemistry calculation, with the partial charges derived using the distributed multipole analysis method [45]. Fe was simulated using the many-body embedded-atom potential [46]. In the case of CO_2, the electrostatic interactions were evaluated using the smooth particle mesh Ewald method. The MD systems were first equilibrated in the constant pressure and temperature ensemble at respective state points for 20 ps. System properties were subsequently simulated at different temperatures and averaged in the constant energy and volume ensemble for 30 ps.

We are interested in the properties of real dense strongly interacting liquids with potential energy comparable to kinetic energy, and hence we have chosen fairly high densities: $\rho = 1.5$ and 1.9 g/cm^3 for Ar, $\rho = 8$ and 11 g/cm^3 for Fe, and $\rho = 1.34$ g/cm^3 for CO_2. The lowest temperature in each simulation was the melting temperature at the corresponding density, T_m. The highest temperature significantly exceeded the temperature at the Frenkel line at the corresponding density, T_F, taken from the earlier calculation of the Frenkel line in Ar [14], Fe [47], and CO_2 [48]. As discussed above, the temperature range between T_m and T_F corresponds to the regime where transverse modes progressively disappear and where Eq. (2) applies. We have simulated 100–700 temperature points at each pressure depending on the system. The number of temperature points was chosen to keep the temperature step close to 10 K.

As discussed above, Eq. (2) applies to subcritical liquids as well as to supercritical fluids below the Frenkel line. Accordingly, our simulations include the temperature range both below and above the critical temperature. This will be discussed in more detail below.

IV. RESULTS AND DISCUSSION

A. Liquid energy and heat capacity

We have calculated ω_F in (2) from its definition in (1), as $\omega_F = \frac{1}{\tau}$. τ can be calculated in a number of ways. Most common methods calculate τ as the decay time of the self-intermediate scattering or other functions by the factor of e or as the time at which the mean-squared displacement crosses over from the ballistic to the diffusive regime [49]. These methods give τ in agreement with a method employing the overlap function depending on the cutoff parameter a_c provided $a_c = 0.3a$, where a is the intermolecular distance [49]. We use the latter method and calculate τ at 13–20 temperature points at each density depending on the system. At each density, we fit τ to the commonly used Vogel-Fulcher-Tammann dependence and use $\omega_F = \frac{1}{\tau}$ to calculate the liquid energy predicted from the theory. The predicted c_v is calculated as $c_v = \frac{1}{N}\frac{dE}{dT}$, where E is given by Eq. (2):

$$c_v = 3 - \left(\frac{\omega_F}{\omega_D}\right)^3 - \frac{3T\omega_F^2}{\omega_D^3}\frac{d\omega_F}{dT}, \quad (3)$$

where N is the number of atoms for Ar and Fe and the number of molecules for CO_2.

The first two terms in (3) give $c_v = 2$ when ω_F tends to its high-temperature limit of ω_F. The last term reduces c_v below 2 by a small amount because $\frac{d\omega_F}{dT}$ is close to zero at high temperature [17].

We now compare the calculated energy and c_v with those directly computed in the MD simulations. We note that the energy in Eq. (2) is the energy of thermal phonon motion, E_T, which contributes to the total liquid energy as

$$E = E_0 + E_T, \quad (4)$$

where E_0 is the liquid energy at zero temperature and represents the temperature-independent background contribution due to the interaction energy.

In comparing the calculated E_T in Eq. (2) with the energy from MD simulations, we therefore subtract the constant term from the MD energy. The comparison of $c_v = \frac{1}{N}\frac{dE}{dT}$ is performed directly because the constant term does not contribute to c_v. We have also calculated c_v using the fluctuations formula for the kinetic energy K in the constant energy ensemble: $\langle K^2\rangle - \langle K\rangle^2 = 1.5(k_BT)^2N(1 - 1.5k_B/c_v)$ [50]. Both methods agree well, as follows from Figs. 2(a) and 2(b).

There is only one adjustable parameter in Eq. (2), ω_D, which is expected to be close to the transverse Debye frequency. ω_F is independently calculated from the MD simulation as discussed above. In Figs. 2 and 3, we compare the energy and c_v calculated on the basis of Eqs. (2) and (3), and we compare them with those computed in MD simulations. The blue circle in each figure shows the critical temperature. We observe good agreement between predicted and calculated properties in a temperature range including both subcritical and supercritical temperature. This involved using $\tau_D \approx 0.6$ ps ($\rho = 8$ g/cm^3) and $\tau_D \approx 0.2$ ps ($\rho = 11$ g/cm^3) for Fe, $\tau_D \approx 0.9$ ps ($\rho = 1.5$ g/cm^3) and $\tau_D \approx 0.3$ ps ($\rho = 1.9$ g/cm^3) for Ar, and $\tau_D \approx 0.5$ ps for CO_2, in reasonable order-of-magnitude agreement with experimental τ_D of respective crystalline systems as well as maximal frequencies seen in experimental liquid dispersion curves (see, e.g., [26]). We note that the expected trend of τ_D reduces with density.

At high temperature where $\omega_F \approx \omega_D$, Eq. (3) predicts c_v close to 2, noting that the last term gives only a small contribution to c_v because ω_F becomes slowly varying at high temperature. Consistent with this prediction, we observe the decrease of c_v from 3 to 2 in Figs. 2 and 3.

The agreement between the predicted and calculated results supports the interpretation of the decrease of c_v with temperature discussed in the Introduction: ω_F decreases with temperature, and this causes a reduction in the number of transverse modes propagating above ω_F and hence the reduction of c_v.

For CO_2, the same mechanism operates except that we need to account for degrees of freedom in a molecular system. We first consider the case of solid CO_2. The MD interatomic potential treats CO_2 molecules as rigid linear units, contributing the kinetic term of 2.5 to the specific heat per molecule, including 1 from the rotational degrees of freedom of the linear molecular and 1.5 from translations (here, we have noted that CO_2 molecules librate and rotate in the solid at low and high temperature, respectively [51]). Noting that the potential energy contributes the same term due to equipartition,

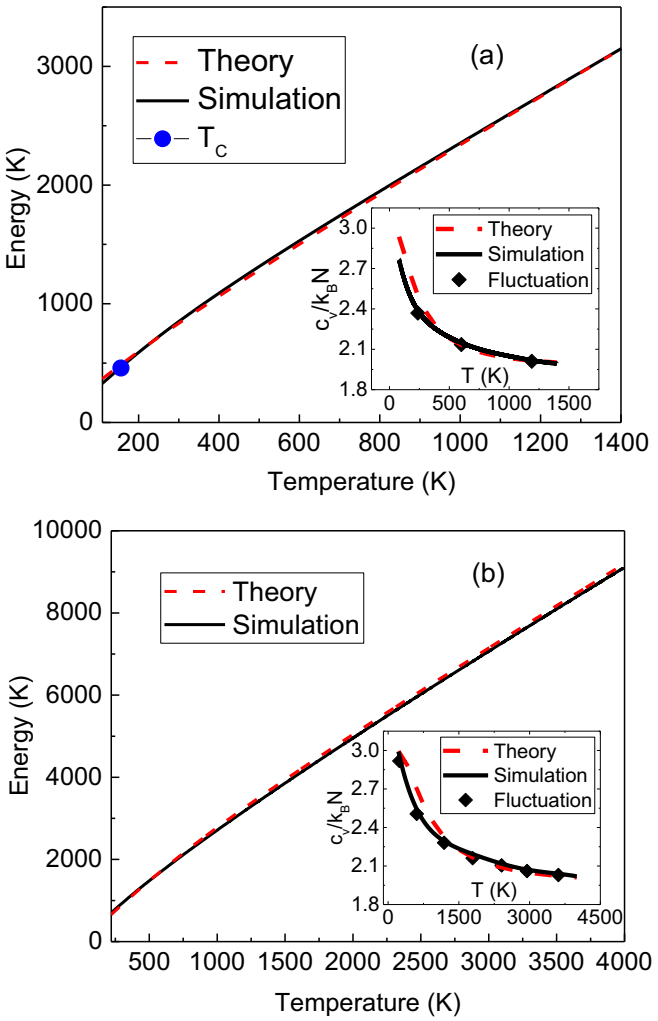

FIG. 2. Energy per particle and specific heat of Ar at density $\rho = 1.5$ g/cm^3 (a) and $\rho = 1.9$ g/cm^3 (b). Solid and dashed lines correspond to results from simulations and theory, respectively. The large (blue) circle corresponds to critical temperature. The black solid curves in the insets show c_v calculated as $c_v = \frac{1}{N}\frac{dE}{dT}$. Solid diamonds correspond to c_v calculated from the fluctuation formula (see the text). The red (dashed) line is the theoretical result for c_v.

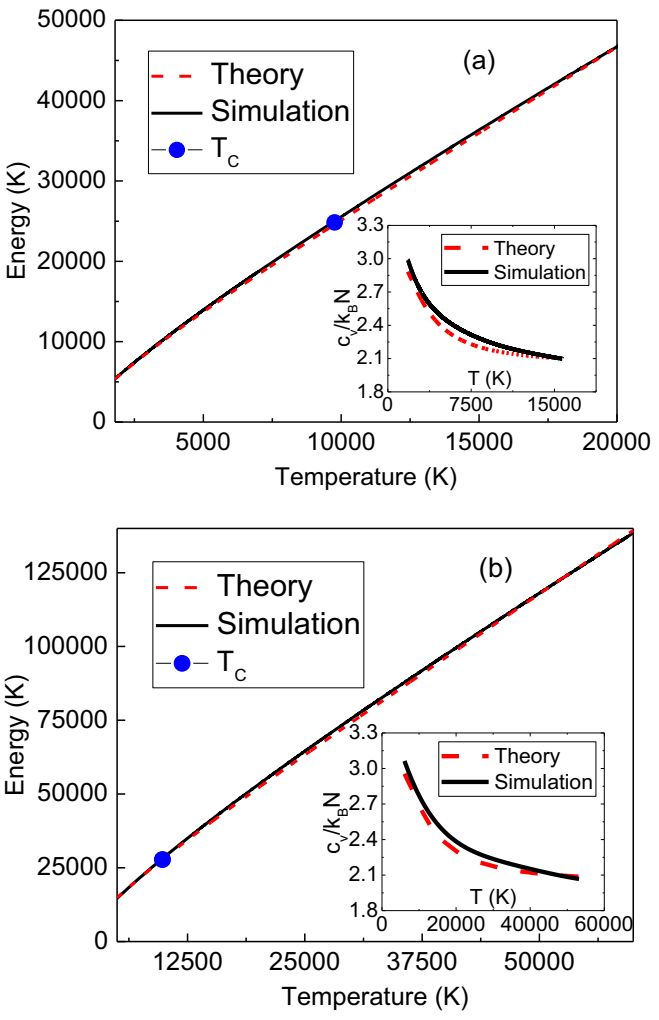

FIG. 3. Energy per particle and specific heat of Fe at density $\rho = 8$ g/cm^3 (a) and $\rho = 11$ g/cm^3 (b). Solid and dashed lines correspond to results from simulations and theory, respectively. The large (blue) circle corresponds to critical temperature. The black solid curves in the insets show c_v calculated as $c_v = \frac{1}{N}\frac{dE}{dT}$. The red (dashed) line is the theoretical result for c_v.

the specific heat becomes 5 per molecule. This implies that for molecular CO_2, Eq. (2) modifies as $E_T = NT[5 - (\frac{\omega_F}{\omega_D})^3]$, where N is the number of molecules and ω_F is related to the jump frequency of molecules and which gives $c_v = 5$ in the solid state where ω_F is infinite. We use the modified equation to calculate the energy and c_v and compare them to those computed from the MD simulation in Fig. 4.

Consistent with the above discussion, we observe that c_v for CO_2 calculated directly from the MD simulations is close to 5 at low temperature just above melting. At this temperature, $\omega_F \ll \omega_D$, giving the solidlike value of c_v as in the case of monatomic Ar and Fe. As temperature increases, two transverse modes of intermolecular motion progressively disappear, resulting in the decrease of c_v to the value of about $c_v = 4$, in agreement with c_v calculated from the theoretical equation for E_T.

We note that the temperature range in which we compare the predicted and calculated properties is notably large (e.g., 200–8000 K for Ar and 2000–55 000 K for Fe). This range is 10–100 times larger than those typically considered earlier [17]. The higher temperatures for Fe might seem unusual, however we note that liquid iron as well as supercritical iron fluid remains an unmodified system up to very high temperature: the first ionization potential of Fe is 7.9 eV, or over 90 000 K. Hence the considered temperature range is below the temperature at which the system changes its structure and type of interactions.

The very wide temperature range reported here is mostly related to the large part of the temperature interval in Figs. 2–4 being above the critical point where no phase transition intervenes and where the liquid phase exists at high temperature, in contrast to subcritical liquids where the upper temperature is limited by the boiling line. The agreement between predicted and calculated properties in such a wide

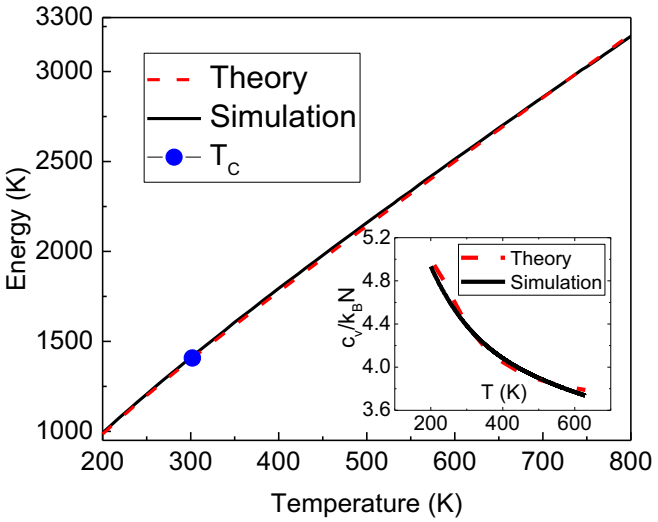

FIG. 4. Energy per particle and specific heat of CO_2 at density $\rho = 1.34$ g/cm^3. Solid and dashed lines correspond to results from simulations and theory, respectively. The large (blue) circle corresponds to critical temperature. The black solid curves in the insets show c_v calculated as $c_v = \frac{1}{N}\frac{dE}{dT}$. The red (dashed) line is the theoretical result for c_v.

temperature range adds support to the phonon approach to liquid thermodynamics we propose.

We make three points regarding the observed agreement between the calculated and predicted results. First, the collective modes contributing to the thermal energy in (2) are considered to be harmonic. The anharmonicity can be accounted for in the Grüneisen approximation, however this involves an additional parameter [17]. We attempted to avoid introducing additional parameters and sought to test Eq. (2), which contains only one parameter, ω_D.

Second, Eq. (2) involves the Debye model and quadratic density of states (DOS). This approximation is justified since the Debye model is particularly relevant for disordered isotropic systems such as glasses [12], which are known to be nearly identical to liquids from a structural point of view. Furthermore, the experimental dispersion curves in liquids are very similar to those in solids such as polycrystals [27–29]. Therefore, the Debye model can be used in liquids to the same extent as in solids. One important consequence of this is that the high-frequency range of the phonon spectrum makes the largest contribution to the energy, as it does in solids including disordered solids. We also note that the liquid DOS can be represented as the sum of solidlike and gaslike components in the two-phase thermodynamic model [52], and the solidlike component can be extracted from the liquid DOS calculated in MD simulations. This can provide more information about the DOS beyond the Debye approximation.

Third, Eq. (2) assumes a lower-frequency cutoff for transverse waves, $\omega_F = \frac{1}{\tau}$, as envisaged by Frenkel in (1). Our recent detailed analysis of the Frenkel equations shows that the dispersion relationship for liquid transverse modes is $\omega = \sqrt{c_s^2 k^2 - \frac{1}{4\tau^2}}$, where c_s is the shear speed of sound and k is the wave number [17]. Here, ω gradually crosses over from 0 to its solidlike branch $\omega = c_s k$ when $\omega \gg \omega_F = \frac{1}{\tau}$.

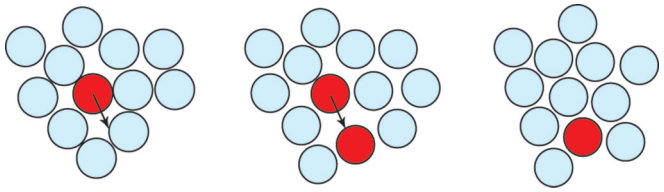

FIG. 5. Schematic representation of a jump event in the liquid.

In this sense, using a lower-frequency cutoff in (2) might be thought of as an approximation. However, we have recently shown [53] that the square-root dependence of ω on τ gives the liquid energy that is identical to (2).

B. Structural crossover and its relationship to dynamical and thermodynamic properties

The results in the previous sections support the picture in which the decrease of liquid c_v from 3 to 2 is related to a reduction of the energy of transverse modes propagating above ω_F as described by Eq. (3). According to Eq. (3), $c_v = 2$ corresponds to the complete disappearance of transverse modes at the FL when $\omega_F \approx \omega_D$ (the disappearance is supported by the direct calculation of transverse modes on the basis of current correlation functions [42]). Importantly, $c_v = 2$ marks the crossover of c_v because the evolution of collective modes is qualitatively different below and above the FL [17]. Below the line, transverse modes disappear starting from the lowest frequency ω_F. Above the line, the remaining longitudinal mode starts disappearing starting from the highest frequency $\frac{2\pi c}{L}$, where L is the particle mean free path (no oscillations can take place at distance smaller than L). This gives qualitatively different behavior of the energy and c_v below and above the FL, resulting in their crossover at the FL [17].

Interestingly, the thermodynamic crossover at $c_v = 2$ implies a structural crossover. Indeed, the energy per particle in a system with pairwise interactions is

$$E = \frac{3}{2}k_B T + 4\pi\rho \int_0^\infty r^2 U(r) g(r) dr, \qquad (5)$$

where $\rho = N/V$ is the number density and $g(r)$ is a radial distribution function.

According to Eq. (4), the liquid energy is $E = E_0 + E_T$, where E_T is given by Eq. (2). If the system energy undergoes the crossover at the FL where $c_v = 2$, Eq. (5) implies that $g(r)$ should also undergo a crossover. Therefore, the structural crossover in liquids can be predicted on the basis of the thermodynamic properties.

We also expect the structural crossover at the FL to be related to the dynamical crossover on general grounds. As discussed above, below the FL particles oscillate around quasiequilibrium positions and occasionally jump between them. The average time between jumps is given by liquid relaxation time, τ. (Figure 5 schematically shows a local jump event from its surrounding "cage.") This means that a static structure exists during τ for a large number of particles below the FL, giving rise to the well-defined medium-range order comparable to that existing in disordered solids [54]. On the other hand, the particles lose the oscillatory component of motion above the FL and start to move in a purely diffusive

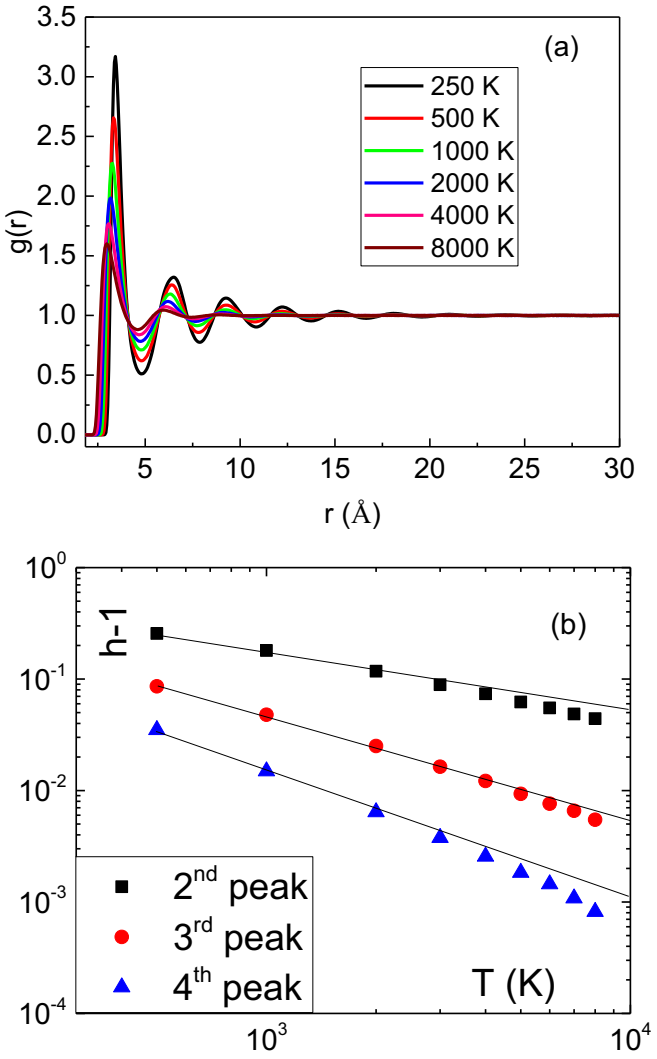

FIG. 6. (a) Pair distribution functions of Ar at different temperatures. The temperatures correspond to the first peak decreasing from top to bottom at 250, 500, 1000, 2000, 4000, and 8000 K; (b) $h-1$, where h are the heights of PDF peaks at different temperatures. The lines are linear fits to the low-temperature data range.

manner as in gases. This implies that the features of $g(r)$ are expected to be gaslike. As a result, $g(r)$ medium-range peaks are expected to have a different temperature dependence below and above the FL. This behavior was observed in Ar in MD simulations in the short-range structure [55]. More recently, the crossover in supercritical Ne in the medium range at the FL was ascertained on the basis of x-ray scattering experiments [56].

In Fig. 6(a) we plot pair distribution functions (PDFs) of Ar at density $\rho = 1.9$ g/cm^3 in a wide temperature range. Using the FL criterion $c_v = 2$ gives the temperature at the FL, T_F, of about 4000 K at that density, which we find to be consistent with the criterion of the disappearance of the minimum of the velocity autocorrelation function [14]. The PDF was calculated with a distance step of 0.05 Å, giving 600 PDF points.

We observe PDF peaks in medium-range order up to about 20 Å at low temperature. The peaks reduce and broaden with temperature. To study this in more detail, we plot the peak heights versus temperature in Fig. 6(b). We observe that the medium-range third and fourth peaks persist well above the critical temperature ($T_c = 151$ K for Ar): the highest temperature simulated corresponds to $53T_c$. Interestingly, this differs from the traditional expectation that the structure of the matter so deep in the supercritical state has gaslike features only. At a temperature above T_F, the height of the fourth peak becomes comparable to its temperature fluctuations (calculated as the standard deviation of the peak height over many structures separated in time by 1 ps at each temperature) by an order of magnitude. The fifth- and higher-order peaks disappear before the highest temperature in the simulated range is reached.

We plot the peak heights in Fig. 6(b) in the double-logarithmic plot because we expect to see an approximate power-law decay of the peak heights at low temperature. Indeed, the PDF in solids can be represented as a set of Gaussian functions with peaks heights h depending on temperature as $h \propto \frac{1}{\sqrt{T}} \exp(-\frac{\alpha}{T})$, where α is a temperature-independent factor [1,57]. This temperature dependence of h was also quantified in MD simulations [58]. h decreases mostly due to the factor $\frac{1}{\sqrt{T}}$, whereas the effect of the exponential factor on h is small and serves to reduce the rate at which h decreases [58]. This implies that in solids, $\log h \propto -\log T$ approximately holds.

In liquids, we expect the same relationship to hold below the FL where $\tau \gg \tau_D$, corresponding to a particle oscillating many times before diffusively moving to the next quasi-equilibrium position. Indeed, the ratio of the number of diffusing particles N_{dif} to the total number of particles N in the equilibrium state is $\frac{N_{dif}}{N} = \frac{\tau_D}{\tau}$ [17] at any given moment of time. $\frac{N_{dif}}{N}$ is small when $\tau \gg \tau_D$ below the FL and can be neglected. Hence, $\log h \propto -\log T$ applies to liquids at any given moment of time below the FL where $\tau \gg \tau_D$. This also applies to longer observation times if h is averaged over τ [17]. We note that the above result, $h \propto \frac{1}{\sqrt{T}}$, involves the assumption that the energy of particle displacements is harmonic (see, e.g., Ref. [1]). Anharmonicity becomes appreciable at high temperature, however the anharmonic energy terms are generally small compared to the harmonic energy. This is witnessed by the closeness of high-temperature c_v to its harmonic result for both solids and high-temperature liquids [59,60].

We therefore expect that $\log(h-1) \propto -\log T$ approximately holds in the low-temperature range below the FL as in solids but deviates from the linearity around the crossover at the FL where $\tau \to \tau_D$ and where the dynamics becomes gaslike [the calculated PDF in Fig. 6(a) is normalized to 1 where no correlations are present at large distances; hence we plot $h-1$ in order to compare it with the theoretical result $h \propto \frac{1}{\sqrt{T}}$, which tends to zero when no correlations are present at high temperature]. We note that the crossover is expected to be broad because $\tau \gg \tau_D$ applies well below the FL only. A substantial diffusive motion takes place in the vicinity of the line where $\frac{N_{dif}}{N}$ cannot be neglected, affecting the linear relationship.

Consistent with the above prediction, we observe the linear regime at low temperature in Fig. 6(b), followed by the deviation from the straight lines taking place around 3000 K for the second peak, 5000 K for the third peak, and 4000 K for the fourth peak, respectively. The smooth crossover in the

3000–5000 K range is centered around 4000 K, consistent with the temperature at the Frenkel line discussed above. We also note that 4000 K corresponds to the specific heat $c_v = 2$ in Fig. 2(b), in agreement with the earlier discussion.

V. SUMMARY

As discussed in the Introduction, liquids have been viewed as inherently complicated systems lacking useful theoretical concepts such as a small parameter [12]. Together with recent experimental evidence and theory [17], the modeling data presented here and its quantitative agreement with predictions are beginning to change this traditional perspective. Our extensive molecular-dynamics simulations of liquid energy and specific heat provide direct evidence for the link between the dynamical and thermodynamic properties of liquids. We have found this to be the case for several important types of liquids at both subcritical and supercritical conditions spanning thousands of degrees Kelvin. This supports an emerging picture that liquid thermodynamics can be understood on the basis of high-frequency collective modes. A more general implication is that, contrary to the prevailing view, liquids are emerging as systems amenable to theoretical understanding in a consistent picture, as is the case in solid-state theory. In addition to the link between dynamical and thermodynamic properties, we have discussed how these properties are related to liquid structure.

ACKNOWLEDGMENTS

This research utilized MidPlus computational facilities supported by QMUL Research-IT and funded by the EPSRC Grant No. EP/K000128/1. We acknowledge the support of the Royal Society, RFBR (15-52-10003), and CSC.

[1] J. Frenkel, *Kinetic Theory of Liquids* (Oxford University Press, Oxford, 1947).
[2] J. P. Boon and S. Yip, *Molecular Hydrodynamics* (Courier Dover, New York, 1980).
[3] N. H. March, *Liquid Metals* (Cambridge University Press, Cambridge, 1990).
[4] N. H. March and M. P. Tosi, *Atomic Dynamics in Liquids* (Dover Publications, Richmond, TX, 1991).
[5] S. Chapman and T. G. Cowling, *The Mathematical Theory of Non-uniform Gases* (Cambridge University Press, Cambridge, 1995).
[6] U. Balucani and M. Zoppi, *Dynamics of the Liquid State* (Oxford University Press, Oxford, 1995).
[7] J. M. Ziman, *Models of Disorder* (Cambridge University Press, Cambridge, 1995).
[8] R. Zwanzig, *Non-Equilibrium Statistical Mechanics* (Oxford University Press, Oxford, 2001).
[9] J. L. Barrat and J. P. Hansen, *Basic Concepts for Simple and Complex Fluids* (Cambridge University Press, Cambridge, 2003).
[10] T. E. Faber, *Introduction to the Theory of Liquid Metals* (Cambridge University Press, Cambridge, 2010).
[11] J. P. Hansen and I. R. McDonald, *Theory of Simple Liquids* (Elsevier, Amsterdam, 2013).
[12] L. D. Landau and E. M. Lifshitz, *Statistical Physics* (Pergamon, Oxford, New York, 1969).
[13] V. V. Brazhkin, Yu. D. Fomin, A. G. Lyapin, V. N. Ryzhov, and K. Trachenko, Phys. Rev. E **85**, 031203 (2012).
[14] V. V. Brazhkin, Yu. D. Fomin, A. G. Lyapin, V. N. Ryzhov, E. N. Tsiok, and K. Trachenko, Phys. Rev. Lett. **111**, 145901 (2013).
[15] G. Grimvall, Phys. Scr. **11**, 381 (1975).
[16] D. C. Wallace, Phys. Rev. E **57**, 1717 (1998).
[17] K. Trachenko and V. V. Brazhkin, Rep. Prog. Phys. **79**, 016502 (2016).
[18] L. D. Landau and E. M. Lifshitz, *Fluid Mechanics* (Pergamon Press, Oxford, New York, 1987).
[19] J. R. D. Copley and J. M. Rowe, Phys. Rev. Lett. **32**, 49 (1974).
[20] W. C. Pilgrim, S. Hosokawa, H. Saggau, H. Sinn, and E. Burkel, J. Non-Cryst. Solids **250-252**, 96 (1999).
[21] E. Burkel, Rep. Prog. Phys. **63**, 171 (2000).
[22] W. C. Pilgrim and C. Morkel, J. Phys.: Condens. Matter **18**, R585 (2006).
[23] T. Scopigno, G. Ruocco, and F. Sette, Rev. Mod. Phys. **77**, 881 (2005).
[24] G. Ruocco and F. Sette, J. Phys.: Condens. Matter **11**, R259 (1999).
[25] S. Hosokawa, M. Inui, Y. Kajihara, K. Matsuda, T. Ichitsubo, W. C. Pilgrim, H. Sinn, L. E. González, D. J. González, S. Tsutsui, and A. Q. R. Baron, Phys. Rev. Lett. **102**, 105502 (2009).
[26] S. Hosokawa, M. Inui, Y. Kajihara, S. Tsutsui, and A. Q. R. Baron, J. Phys.: Condens. Matter **27**, 194104 (2015).
[27] V. M. Giordano and G. Monaco, Proc. Natl. Acad. Sci. (USA) **107**, 21985 (2010).
[28] V. M. Giordano and G. Monaco, Phys. Rev. B **84**, 052201 (2011).
[29] S. Hosokawa *et al.*, J. Phys.: Condens. Matter **25**, 112101 (2013).
[30] A. Cunsolo *et al.*, J. Chem. Phys. **114**, 2259 (2001).
[31] G. G. Simeoni *et al.*, Nat. Phys. **6**, 503 (2010).
[32] M. Grimsditch, R. Bhadra, and L. M. Torell, Phys. Rev. Lett. **62**, 2616 (1989).
[33] F. Scarponi, L. Comez, D. Fioretto, and L. Palmieri, Phys. Rev. B **70**, 054203 (2004).
[34] E. Pontecorvo, M. Krisch, A. Cunsolo, G. Monaco, A. Mermet, R. Verbeni, F. Sette, and G. Ruocco, Phys. Rev. E **71**, 011501 (2005).
[35] A. Cunsolo, C. N. Kodituwakku, F. Bencivenga, M. Frontzek, B. M. Leu, and A. H. Said, Phys. Rev. B **85**, 174305 (2012).
[36] K. Trachenko, Phys. Rev. B **78**, 104201 (2008).
[37] A. R. Dexter and A. J. Matheson, Trans. Faraday Soc. **64**, 2632 (1968).
[38] D. C. Wallace, Phys. Rev. A **25**, 3290 (1982).
[39] F. Puosi and D. Leporini, J. Chem. Phys. **136**, 041104 (2012).
[40] V. V. Brazhkin and K. Trachenko, Phys. Today **65**(11), 68 (2012).
[41] V. V. Brazhkin, A. G. Lyapin, V. N. Ryzhov, K. Trachenko, Yu. D. Fomin, and E. N. Tsiok, Phys. Usp. **55**, 1061 (2012).
[42] Yu. D. Fomin, V. N. Ryzhov, E. N. Tsiok, V. V. Brazhkin, and K. Trachenko, J. Phys.: Condens. Matter **28**, 43LT01 (2016).
[43] I. T. Todorov, B. Smith, M. T. Dove, and K. Trachenko, J. Mater. Chem. **16**, 1911 (2006).

[44] J. L. Yarnell, M. J. Katz, R. G. Wenzel, and S. H. Koenig, Phys. Rev. A **7**, 2130 (1973).
[45] M. Gao, A. M. Misquitta, C. Yang, I. T. Todorov, A. Mutters, and M. T. Dove (unpublished); M. Gao, Ph.D. thesis, Queen Mary University of London (unpublished).
[46] A. B. Belonoshko, R. Ahuja, and B. Johansson, Phys. Rev. Lett. **84**, 3638 (2000).
[47] Y. Fomin *et al.*, Sci. Rep. **4**, 7194 (2014).
[48] C. Yang, V. V. Brazhkin, M. T. Dove, and K. Trachenko, Phys. Rev. E **91**, 012112 (2015).
[49] S. Sengupta, F. Vasconcelos, F. Affouard, and S. Sastry, J. Chem. Phys. **135**, 194503 (2011).
[50] D. Frenkel and B. Smit, *Understanding Molecular Simulation: From Algorithms to Applications* (Academic Press, San Diego, San Francisco, 2001).
[51] S. Liu, M. A. Doverspike, and M. S. Conradi, J. Chem. Phys. **81**, 6064 (1984).
[52] S.-T Lin, M. Blanco, and W. A. Goddard III, J. Chem. Phys. **119**, 11792 (2003).
[53] C. Yang *et al.* (unpublished).
[54] P. S. Salmon, R. A. Martin, P. E. Mason, and G. J. Cuello, Nature (London) **435**, 75 (2005).
[55] D. Bolmatov, V. V. Brazhkin, Yu. D. Fomin, V. N. Ryzhov, and K. Trachenko, J. Chem. Phys. **139**, 234501 (2013).
[56] C. Prescher *et al.*, arXiv:1608.08437.
[57] A. A. Maradudin, E. W. Montroll, G. H. Weiss, and I. P. Ipatova, *Theory of Lattice Dynamics in the Harmonic Approximation* (Academic, New York, 1971).
[58] S. O. Yurchenko, N. P. Kryuchkov, and A. V. Ivlev, J. Chem. Phys. **143**, 034506 (2015).
[59] E. I. Andritsos *et al.*, J. Phys.: Condens. Matter **25**, 235401 (2013).
[60] D. Bolmatov and K. Trachenko, Phys. Rev. B **84**, 054106 (2011).